New insights into the early stage intercalation mechanism in carbon based anode materials.†

Jafar Azizi,*,† Axel Groß,*,† and Holger Euchner*,‡

†*Institute of Theoretical Chemistry, Ulm University, D-89081 Ulm, Germany*

‡*Institute of Physical and Theoretical Chemistry, Tübingen University, 72076 Tübingen, Germany*

E-mail: jafar-1.azizi-shoushbolaghi@uni-ulm.de; axel.gross@uni-ulm.de; holger.euchner@uni-tuebingen.de

Abstract

Graphite and graphite derivatives, the standard anode materials for Li-ion batteries, are also of great interest for post-Li ion technologies such as K-ion batteries. However, certain aspects of the intercalation process in these systems as well as the resulting consequences still require a deeper understanding. In particular, the first steps of the K intercalation in graphitic systems, i.e. at low concentrations, are fundamentally different from the case of Li. Herein, we use density functional theory to elucidate the early stage intercalation of K in graphitic materials by seeking comparison to the behaviour of Li and Na. Our results show the crucial role of the competition between the interlayer van der Waals interaction and the covalent AM-C bonds for the initial Li-, Na-, and K-intercalation and mobility in graphitic materials. We identify the first steps of K-intercalation as potential reasons for performance loss and battery failure and show that heteroatom doping can open pathways for solving these issues.

1 Introduction

The exceptional mechanical, electrical, and thermodynamic properties of two-dimensional (2D) van der Waals (vdW) materials which are typically not seen in their 3D counterparts have sparked a lot of attention in many fields of research. In particular, 2D materials such as graphite and its derivatives, but also for instance dichalcogenides, have become promising electrode components in batteries and energy storage systems.[1–5]

Graphite and derivatives thereof are still the standard option for anodes in commercial lithium-ion batteries (LIBs).[2,6–8] It is well known that graphite can intercalate alkali metal (AM) atoms in between its layered structure with half-filled carbon pz orbitals that are perpendicular to the graphitic planes and can interact with the AM s-orbitals.[9,10] While Li, due to its exceptional behaviour and also small size, intercalates easily in graphitic compounds, the competition between vdW interaction and AM-C bond formation can be challenging for larger AM atoms, in particular for small AM concentrations.[11–14]

The working principle of LIBs on the anode side is based on the intercalation and deintercalation of Li atoms between the layers of graphite. Starting from the pioneering work of Hérold in the 1950s [15] lithium graphite intercalation compounds (Li-GICs) have been extensively investigated. Their structural evolution during intercalation/deintercalation was investigated using different experimental techniques such as X-ray diffraction (XRD), Raman scattering or nuclear magnetic resonance.[16–20] Li-GICs exhibit different compositions and crystal structures[21–24] that can be described by the so-called staging mechanism,[25–28] which refers to the periodic stacking of Li layers between the graphitic planes. The resulting structures are denoted as stage-n compounds, where the index n denotes the number of graphene layers stacked between the (filled) intercalant layers.[21,29,30] According to earlier studies[21,31] GICs undergo a shift from AB- to AA-stacking with increasing AM concentration, when sufficient binding energy is provided to overcome the AB-AA transition. These findings were recently also confirmed for defect-containing GICs.[32] For Li, thermodynamically stable GICs with increased AM content exist up to LiC_6 stoichiometry (corresponding

to stage-I),[2] whereas for sodium, only Na–GICs with low Na concentration have been reported. The thermodynamic instability of the intercalation process for reasonable amounts of Na therefore renders graphite unsuited as anode material for NIBs.[21,32–35] Several studies have addressed this issue, explaining why – despite the chemical similarities of Li and Na – graphite does not properly work for sodium intercalation.[13,29] For the case of K stable GICs with significant AM content are observed and e.g. the stage-I compounds, KC_6 and KC_8, as well as the stage-II and stage-IV compounds, KC_{16}, and KC_{72}, have been reported to be stable,[21] while some studies also indicate additional (meta-) stable stoichiometries .[31] The electrochemical intercalation of potassium into graphite has also been extensively studied by different groups and methods, demonstrating a phase evolution and staging behavior that is comparable to, but distinct from, the case of Li.[31,36–39] While larger differences in the intercalation mechanism have been observed for low AM concentrations, most studies focus on GICs with increased AM concentration. Hence, the early steps of intercalation for K in graphite and the atomistic origin as well as the consequences of the differences compared to Li have not been addressed so far. In the present work we systematically investigated the structure and energetics of the first steps of the AM intercalation process in GICs, by means of density functional theory (DFT) calculations. Based on the computed formation energies, we evaluated the stability of the AM intercalation for decreasing AM concentrations. For this purpose, graphite bulk structures based on different numbers of stacked layers and lateral system sizes were constructed. In order to gain a better understanding of the origin and consequences of the observed differences in early stage K- and Li intercalation, we carefully compared the results for Li and K. Furthermore, to better identify potential trends, Na intercalation was also considered.

Regardless of the stability of the intercalation compounds at high AM concentrations, our simulations show that the initial insertion step is dominated by a competition of vdW interaction and intercalation energy. At low concentration this competition can – depending on the intercalant – result in peculiarities for the intercalation process. In fact, for low concen-

trations of large intercalants such as potassium, the graphitic layers around the AM atoms get strongly curved, resulting in a different initial intercalation mechanism as observed for instance for the small Li atom.

Furthermore, the AM diffusion kinetics was investigated for low AM contents, focusing on the impact of the changes in local geometry. Our results show that an increasing lateral system size, corresponding to a lower intralayer AM concentration, affects the AM atom diffusion, especially for large atoms like K, an effect that has so far not been addressed in literature.

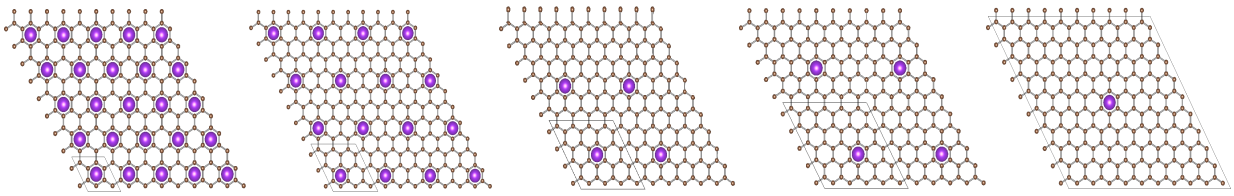

Figure 1: : Schematic representation (projected along the c-axis) of AM intercalation compounds with (a) KC_{16} (b) KC_{36} (C) KC_{64} (d) KC_{100} and (e) KC_{400} stoichiometry. The simulation unit cells are indicated in black.

2 Methods

To investigate the initial stage of the AM intercalation, graphite based model systems have been studied by periodic density functional theory (DFT). For modeling graphitic domains, the investigated bulk systems have been constructed as stacking of graphitic layers. First, different lateral supercell sizes ($AMC_{N\times N\times 2}$ and $AMC_{N\times N\times 3}$, AM= Li, Na, and K and $N = 2..10$) have been constructed to investigate the impact of decreasing AM concentrations. In addition, decreasing AM contents have been probed via structures with increasing layer thickness, corresponding to 2×2×N supercells (with $N = 2..8$).

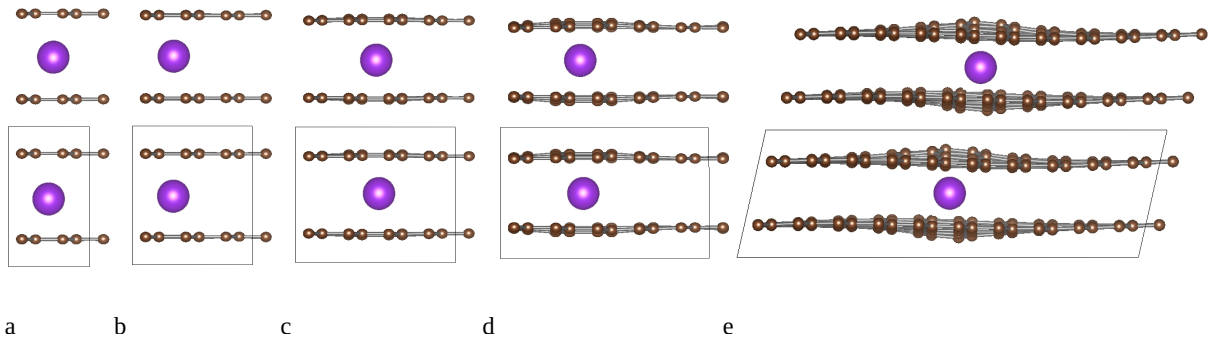

Figure 2: : Schematic representation (side view) of the different supercell sizes used to model the AM-atom intercalation, showing the distortions introduced by K atoms (a) KC_{16} (b) KC_{36} (c) KC_{64} (d) KC_{100} and (e) KC_{400} (corrsponding results for the 3-layer based bulk supercells are shown in Table S1 and Fig. S1 and Fig. S2 in the SI).

All simulations were performed with the Vienna Ab Initio Simulation Package (VASP),[40] using the Projector Augmented Wave (PAW) approach.[41] Exchange and correlation were described via the optPBE functional, which includes a non-local correction scheme to account for van der Waals interactions.[42] The convergence criterion for the self-consistent field (SCF) cycle was set to 10^{-7} eV, while the geometry was optimized until the remaining forces were less than 10^{-3} eV/Å. Each structure was optimized with respect to lattice constant and atomic positions, applying a plane wave cutoff of 600 eV. The structures based on the 2×2×2 (corresponding to C_{16}) supercell were computed with a 10×10×6 k-point mesh, while the other system sizes under investigation were optimized with a corresponding k-point resolution. In order to assess the AM migration, the Nudged Elastic Band (NEB) method[43,44] was applied, with typically five images along the reaction path. For all considered models, rather large system sizes have been chosen to ensure a negligible interaction between the periodic images of the migrating AM-atoms.

3 Results and discussion

Energetics of the intercalation process

Table 1: : Intercalation energy E_{int} (in eV) for Li, Na, and K atoms in the 2-layer based bulk model system with respect to the different supercell sizes/atom concentrations.

Models	C_{16}	C_{36}	C_{64}	C_{100}	C_{144}	C_{196}	C_{256}	C_{324}	C_{400}
Li	-0.21	-0.27	-0.21	-0.21	-0.21	-0.22	-0.20	-0.22	-0.19
Na	0.10	0.25	0.38	0.61	0.59	0.59	0.64	0.64	0.76
K	-0.33	-0.10	0.37	0.87	1.22	1.02	1.11	1.19	1.47

In order to investigate the thermodynamic stability of early stage AM-intercalation, two- and three layer based bulk systems with different AM-atom concentration have been considered as depicted in Fig. 1 and Fig. S1 in the supplementary information (SI). For these systems, the energetic stability of an intercalated single AM atom was investigated by calculating the intercalation energy with respect to the AM–free system:

$$E_{int} = E_{G+AM} - (E_G + E_{AM}) \tag{1}$$

Here, E_{G+AM} is the total energy of the graphitic system after the insertion of one AM atom, and E_G is the energy of the AM-free layers, wheras E_{AM} is the energy of the AM in the bulk metal phase. In the case of Li, the intercalation at low concentration is energetically favorable, yielding an energy gain of ~ -0.2 eV for different AM concentrations in a 2-layer bulk system as depicted in Fig. 3a and Tab. 1. Slightly changing numbers have been obtained for a 3-layer based bulk structure (see Tab. S1 in the SI). Note that the stronger the intercalation in a particular anode material, i.e., the more negative the intercalation energy, the smaller the open circuit voltage of the corresponding battery. However, a certain driving force is needed in order to avoid metal plating at the anode. The fact that Li intercalation is energetically favorable is among other factors a consequence of the small size of the Li atom, resulting only in local distortions around the intercalated ion, with a range that is already covered by small supercell sizes. Here, the small observed fluctuations in

the intercalation energy for increasing system size are due the matching conditions of the introduced distortion with the periodicity of the cell. Regarding K intercalation, on the other hand, significant differences are observed in comparison to Li. The K-atom intercalation also becomes favorable for higher concentrations, however, for increased lateral system size and hence low AM contents – in contrast to the case of Li – it becomes largely unfavorable as depicted in Fig. 3a and Tab. 1. The corresponding results for the 3-layer based bulks system are given in Tab. S1 in the SI. Finally, for Na, it is known that no significant amounts of ions can be intercalated with the intercalation of rather small fractions becoming already thermodynamically unstable. As in the case of K, at very low concentrations the further decrease of the Na content turns the intercalation more and more unfavorable (see Fig. 3a and Tables 1). So, while Li intercalation is essentially independent of the concentration – in the low concentration limit – decreasing the K content to roughly KC_{64} (or less) results in a tremendous change in the intercalation energy for the 2-layer based bulk system. For Na the same effect, however, with a somewhat less pronounced change is observed. Hence, also for very low concentrations there is a significant impact of ion type (and size) on the intercalation process. Indeed, the intercalation of small fractions of Na and K atoms highly affect the geometry of the system, and result in a local curvature around the intercalants, as shown in Fig. 2. Taking a closer look at the geometry of a KC_{400} model structure – i.e. at very low K concentrations – shows that far from the intercalant site the layer distance reaches a value of 3.44 Å, which almost corresponds to that one of pristine graphite, whereas in the vicinity of the intercalant the system is strongly curved (see inset of Fig. 3). In general, decreasing the AM concentration, results in a strong, localized curvature of the graphitic layers around the intercalated atoms, which is a caused by the competition of AM intercalation and inter-plane vdW interactions. While the vdW forces attempt to keep the neighbouring graphitic layers at their equilibrium distance, the intercalants aim at increasing the spacing between the layers. The consequence of these competing forces is that the system minimizes its energy by introducing a curvature into the graphitic layers in the vicinity of the

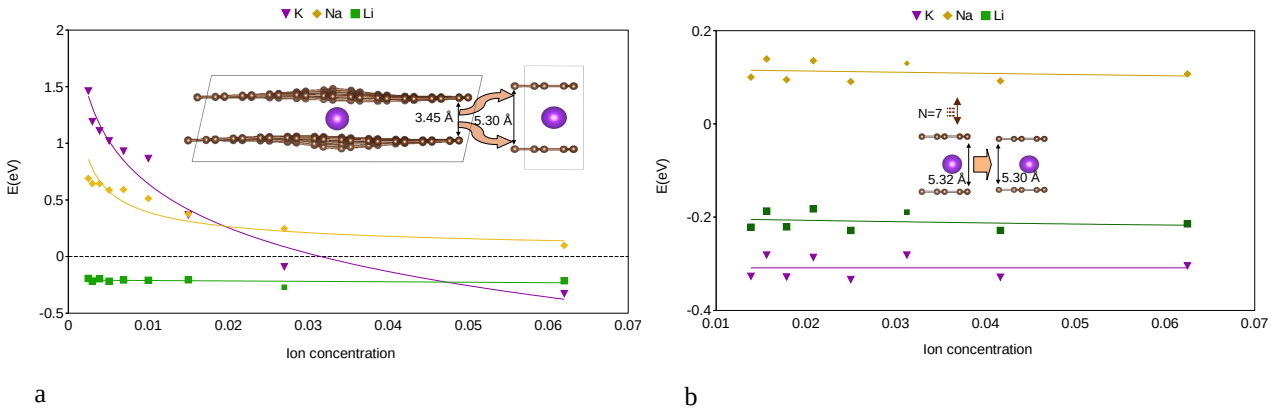

Figure 3: : Intercalation energy E_{int} (in eV) for single AM (Li, Na, and K) atoms as obtained for the 2-layer based bulk system (a) Intercalation energy with respect to the different lateral supercell sizes and hence different AM concentrations (b) Intercalation energy for systems with a different number of stacked layers based on an AMC_{16} cell. The insets show the change in layer distance for the case of K intercalation. The solid lines serve as a guide for the eye.

intercalated ion. The strength of this curvature depends on the ionic radii of the intercalant, hence showing a more pronounced effect for larger AM atoms. Finally, it is crucial to point

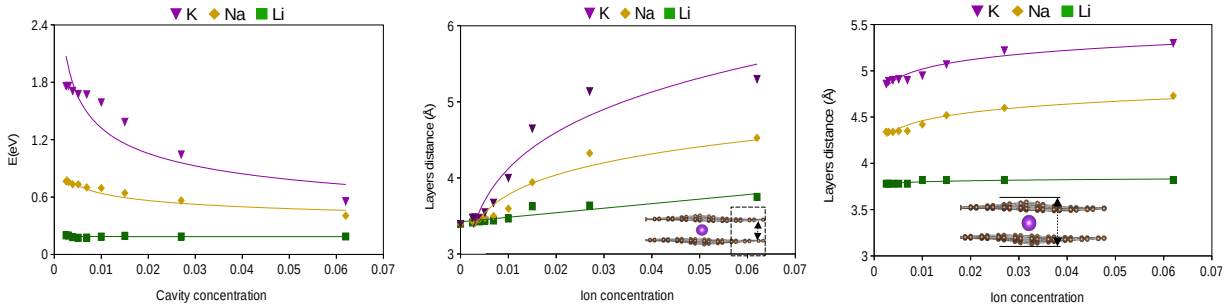

Figure 4: : Graphite layer distance and defect formation energy for different super cell sizes of the 2-layer based bulk system ($AMC_{N\times N\times 2}$, AM= Li, Na, and K, N= 2, 3, ..., 10) (a) defect (curvature) formation energy for different super cell sizes (b) graphite layers distance far from the intercalant (c) layer distance in at the intercalant site.

out again that while the intercalation of K atoms is unfavorable at low concentrations, K intercalation compounds become energetically stable at higher AM content. Thus, a certain K concentration per unit-cell – in the 2-layer based system somewhere between KC_{64}

and KC_{36}) – stabilizes the intercalation, meaning that the energy gain due to K-C bonds compensates the energy penalty for a decreased vdW interaction (see Fig. 3a and Table 1). This indicates that a certain K concentration between two graphitic planes is necessary to stabilize the intercalation process.

To further validate this assumption, we have then investigated the impact of gradually decreasing the AM concentration by increasing the number of carbon layers in the underlying bulk supercell, again starting from the 2-layer based bulk structure. To investigate the AM intercalation, the starting stoichiometry of AMC_{16}, corresponding to one completely filled and one empty AM layer (stage II compound), was chosen. By adding further (empty) carbon layers to the bulk supercell – i.e. the AM concentration in the filled layers remains high – the intercalation energy is in all cases found to reach a constant value (see Fig. 3b). It has to be noted that the AMC_{16} compounds – as is well known from literature – adapt an AA stacking sequence. On the other hand, empty graphitic layers that are added to increase the system size were chosen to follow an AB stacking sequence. Due to the periodic boundary conditions, this means that simulations with an odd number of graphitic layers will have no empty AA stacked layers while those with even layer numbers are forced to have one – energetically less favorable – empty AA stacked layer. Hence, periodic like fluctuations of the formation energy are observed, while the latter one is otherwise not showing considerable changes with increasing number of carbon layers (see Fig. 3,b). This indeed means that the AM concentration per layer is the crucial factor for the K-intercalation. In other words, low K concentrations can only be stably intercalated by locally high K contents within one layer. This differs from the case of Li and leaves the question on how the K intercalation process can be started to some extent open. The energetically unfavourable intercalation of Na and in particular K atoms in graphitic systems at low AM concentrations means that instead of entering the anodes the AM atoms would rather form metallic deposits on the anode surface. This means that plating would occur which could then lead to dendrite growth and fire hazards in a battery.[45] And indeed, plating on graphitic anodes has been observed to

represent a considerable safety issue in sodium ion batteries,[46] but especially in potassium ion batteries.[47] Together with the experimentally observed increased resistance,[31] this can hence be understood as a consequence of the unfavorable energetics at low K concentrations. Consequently, an in-depth understanding of the early stages of AM intercalation is crucial for improving carbon based anodes for KIBs. In the following, we therefore further investigate the reasons for the differences in the (early stage) AM intercalation mechanism as well as the corresponding diffusion kinetics. Finally, we propose strategies to mitigate the energetically (partially) unfavourable Na and K intercalation in graphitic anodes, which may help to promote NIBs and KIBs as efficient and more sustainable alternatives to LIBs.[48]

Cavity formation energy

To further elucidate the differences in the intercalation process for Li, Na and K, we have divided the latter one in two steps. The first step corresponds to the formation of the cavity that is created by the respective AM atom. By calculating the penalty for the formation of this cavity, the energy needed to compensate the vdW interaction can be deduced (see Fig. 4 a). In principle, this energy penalty can be understood as a kind of defect formation energy, which can be computed via the following expression:

$$E_{def} = E_{CG} - E_{PG}, \tag{2}$$

where E_{CG} and E_{PG} represent the total energy of the curved and pristine graphite. As already discussed in the previous sections, the created cavity depends on the size of the intercalant. Consequently, the defect generation energies show a significant variation in energy, based on the alkali metal and its size. Hence, compared to Li, the Na and K cavities result in a much higher defect formation energy. While the defect formation energy for Li is almost constant with respect to the (lateral) supercell size, the defect formation energy for Na is increasing for larger supercells (see Fig. 4a). Finally, the defect formation energy

of the cavity originating from K-interclations is found to be even higher than that of Na, as expected from its larger ionic radius. For both cases the defect formation energies are expected to reach a constant value at low concentrations (i.e. for even larger system sizes), but this point seems not to be reached yet. Furthermore, by determining the maximum and the minimum layer spacing in the considered model system, the extension of the cavity can be quantified For the case of Li, the cavity approaches a constant size when the lateral dimensions of the supercell increase (see Fig. 4b,c), which is in accordance with the defect formation energy being constant. In principle, the same behaviour can be expected for Na and K, however, the extension of the cavity is much larger and as already seen for the defect formation energy this point is not fully reached yet.

Diffusion kinetics

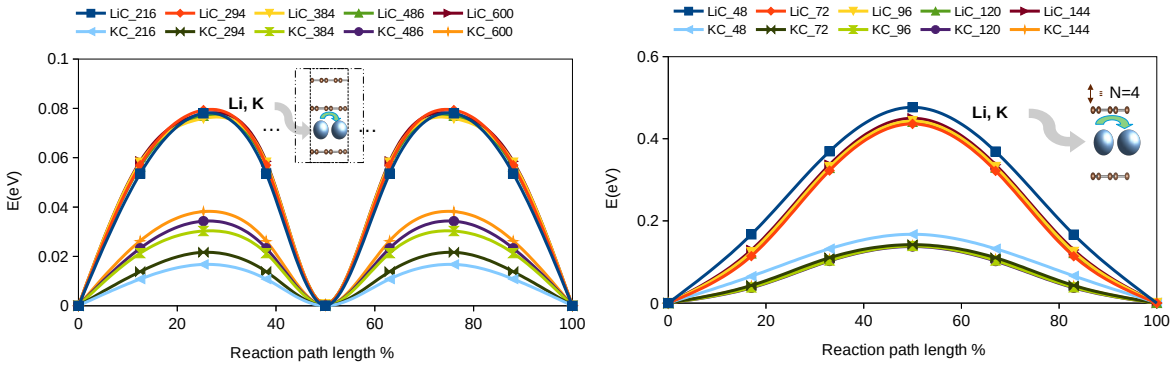

a b

Figure 5: :Minimum energy path (a) for three layer based bulk system with different lateral super cell size ($AMC_{N\times N\times 3}$, AM= Li, K, and $N = 6 - 10$). Two layers that contains the AM atoms are in AB stacking (b) for Li and K diffusion in KC_{48} unit-cell and for different numbers of graphite layers on top of each other. Two layers that contains the AM atoms are in AA stacking.

Apart from a stable intercalation of the AM atoms, their kinetics is also of great importance for battery applications. Hence, in order to gain an atomistic understanding of the

AM kinetics during the charging/discharging process, the energy barriers for K diffusion at different ion concentrations, again also focusing on the early stage intercalation, were calculated and compared to the case of Li by using the Nudged Elastic Band (NEB) method (see Fig. 5). As for the intercalation energies, two types of structures - based on increasing lateral size and number of stacked layers - were taken into consideration in order to comprehend the diffusion mechanism at low AM concentration. For determining the impact of increasing lateral system size (decreasing AM concentration) and hence increasing AM-AM distance, the 3-layer based bulk system was considered. Here, the choice of a 3-layer based supercell with two empty layers is made to ensure that no spurious effects are introduced by periodic boundary conditions.

As the AB-stacked graphite is more favorable for low concentration, we considered a stacking sequence in which the two layers that contain the AM atoms show AB-stacking. It should be noted that while in AA-stacked graphite, the AM atoms are located above/below hollow sites of both upper and lower layer, for AB-stacking the AMs are located at the hollow site of one graphitic layer and on a top site with respect to the other. For the investigated low concentrations, the Li migration barriers amount to less than 0.1 eV and are essentially independent of the lateral system size (see Fig. 5a). For, K the migration barriers are even further reduced, but, show a slight dependence on the lateral system size. The observed impact of system size (and hence K concentration) on the K kinetics can be understood as a consequence of the extension of the introduced distortions. For higher in plane AM concentrations the increased lattice spacing around the AM atom results in more space and hence a lowering of the diffusion barriers (see Fig. 2). For the sake of comparison, we furthermore have investigated the same scenario for the AM atoms residing in between AA-stacked layers. Here, the findings are qualitatively the same, with the Li diffusion barriers being largely independent from the lateral size, whereas for the case of K the barriers again showed a slight increase with the system size (see Fig. S3 in the SI). Yet, it has to be pointed out that the diffusion barriers for the AA-stacked layers are significantly increased,

amounting to 0.395-0.41 eV and 0.15-0.22 eV for Li and K, respectively. Thus, the diffusion of Li and K is strongly enhanced as long as the AB-stacking is dominant.

Finally, the impact of the number of empty graphitic layers on the diffusion barriers of the respective intercalants was investigated. In this scenario, low AM concentrations are again obtained by increasing the number of graphitic layers, while considering one layer with a particular AM content that has already transformed to AA-stacking. Here, starting from a two layer based bulk system with LiC_{48} and KC_{48} stoichiometry, no significant changes are observed for an increasing number of graphite layers as soon as more than three layers are considered (see Fig. 5b). The migration barriers for Li and K amount to 0.43 and 0.14 eV, hence, again confirming the lower barriers for the larger K ions. While it is well known that K-GICs in general show lower diffusion barriers than Li-GICs[27,35,49–52] the reason was typically ascribed to the differences in layer spacing caused by the ion sizes. Interestingly, at low AM concentrations the overall finding that K-ions diffuse much faster remains valid, whereas the layer spacing is only increased locally by the introduced distortion. However, this distortion seems large enough to still facilitate the jump to the neighbouring empty sites

Impact of impurities on the intercalation process

Table 2: : Intercalation energy E_{int} (in eV) for Li, Na, and K atoms in a 2-layer based bulk model system (C_{144}) obtained for different impurities (B, S, Si, OH, and Sn), mono-vacancy defect (MV) and also in pristine graphite (G).

Impurities	B	S	Si	OH	Sn	MV	G
Li	-1.24	-0.31	-1.04	-1.44	-1.91	-1.45	-0.20
Na	-0.52	-0.09	-0.69	-1.09	-1.93	-0.54	0.59
K	-0.05	0.10	-0.27	-0.66	-0.63	-0.33	0.93

As discussed above, the relative strength of vdW interaction and covalent AM-C bonds depend on the lateral size and the corresponding AM concentration. For the case of K, our findings clearly show that the intercalation up to a certain K concentration is energetically unfavourable. Hence, it is anticipated that for the initial intercalation of K in graphite, additional driving forces will be beneficial. One way to provide driving forces for the AM

intercalation is the introduction of structural defects.[32,53] The introduction of heteroatoms, on the other hand, offers an additional way to tailor the carbon framework such that the early steps of intercalation may be facilitated. Therefore, to show how heteroatom doping can affect the energetics of the intercalation process, we considered the impact of different impurities in a 2-layer based C_{144} bulk model system. For this purpose, a few different impurities that are likely to be found in or may easily be added to graphitic systems, including B, OH, S, Si, and Sn,[54–58] were investigated. For all impurities, except for the case of OH, a carbon atom was simply substituted by the doping element. The OH molecule on the other hand was placed on top of a carbon atom, thus forming a C-O-H moiety. It should be noted that the considered structures, apart from negligible distortions, remain AB stacked. To assess the impact of the doping elements the intercalation energy, in analogy to eqn. (1), was determined.

$$E_{int} = E_{def+AM} - (E_{def} + E_{AM}) \tag{3}$$

Here, E_{def+AM} is the total energy of the graphitic (impurity containing) system after the insertion of one AM atom, and E_{def} is the energy of the AM-free layers, whereas E_{AM} is the energy of the AM in the bulk metal phase. In general, the obtained intercalation energies indicate that impurities can stabilize the intercalation at low AM concentrations (see Table 2 and Fig. 6d). In particular the intercalation of Na and K in the low concentration limit, which is unstable for pristine graphite, becomes favorable when impurities are considered Apart from changing the energetics, the impurities also have an impact on the equilibrium location of the AM-atoms. For all cases the intercalated AM-atoms have originally been positioned at the center of a honeycomb that comprises the impurity, denoted by the letter C (see Fig. 6a). This corresponds to the AM positions determined for the pristine graphite, i.e. with the AM on top of the center of a six-ring of one graphene sheet and below a carbon atom of the other.

When B doping is considered the geometry of the system is not significantly affected, due to the comparable atomic sizes of boron and carbon. In fact, B-C bonds (1.48 Å) are only

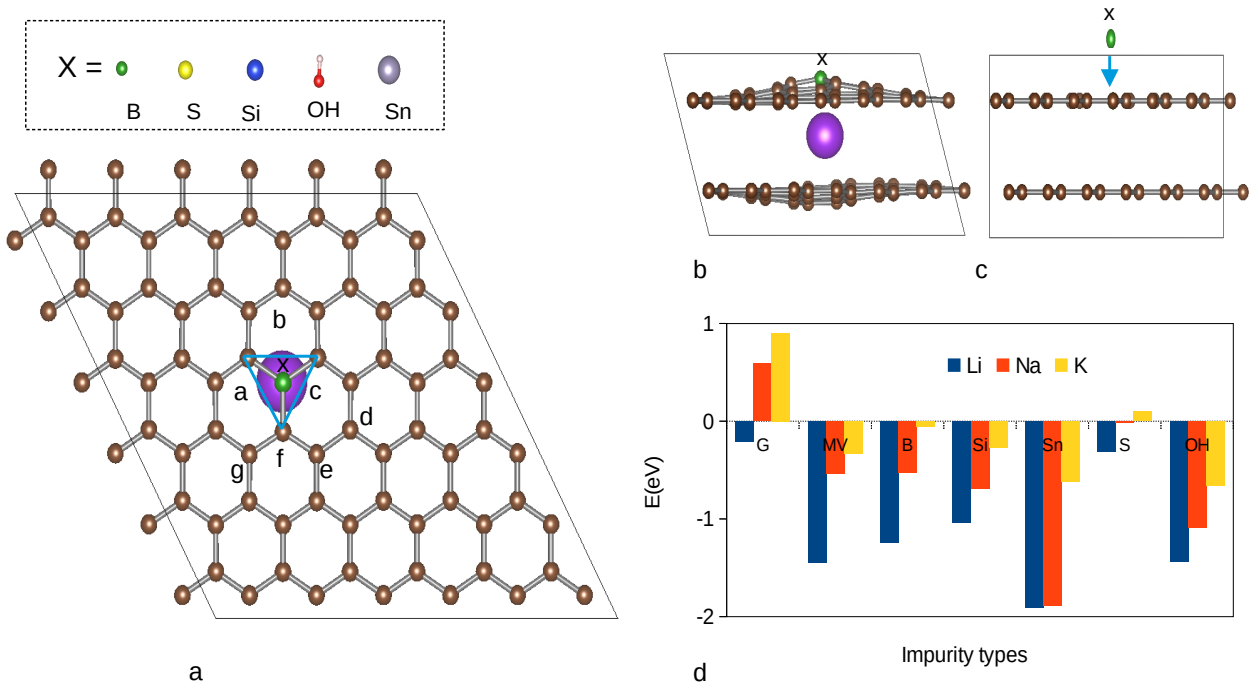

Figure 6: : Different types of impurities in graphics system (a) top view of the graphite (x= B, S, Si, OH, and Sn), while AM-atoms are placed in C site, final possible sites are shown with different alphabets (b) side view of the system after intercalation (c) side view of the system before intercalation (d) intercalation energy Eint (in eV) for Li, Na, and K atoms in 2-layers model (C144) near to the impurity sites (see Table 2), G is the pristine graphite without defect and impurity.

slightly increased as compared to C-C bonds (1.43 Å) in pristine graphite. The AM intercalation process on the other hand is significantly stabilized by the presence of boron, such that Na (-0.52 eV), and K (-0.05 eV) intercalation also become energetically favorable. This stabilization is related to the interaction of boron and the intercalants. In the case of Na and K, the AM atoms prefer to sit on top of the B-impurity, while for the Li atom the C site (hexagon, beside the impurity) is more favorable. Whereas the intercalant-free system is essentially undistorted, the intercalation of AM atoms results in a curving of the graphitic plains as in the case of pristine graphite. This is a also visible in the increased B-C bond length which amounts to 1.49 Å, 1.51 Å, and 1.51 Å for Li, Na and K, respectively. By introducing Si as an impurity, the graphitic plains get slightly curved, which is a consequence of the increased atomic size of Si as compared to C. In addition, a change in bond length

is observed, with the Si-C bonds (1.72 Å) being longer than a pristine C-C bond. Despite the fact that Si and C have the same valence, the intercalated AM-atoms migrate to the top of the impurity, while they are at the center of a hexagon in the adjacent layer. The Si-C bonds further increase from 1.72 Å in the intercalant-free system to 1.77 - 1.78 Å for AM intercalation. As for the pristine and B-doped system the curvature after intercalation scales with the AM size. From the energetic point of view, the AM intercalation is stabilized by the Si impurity with K and Na again showing a negative intercalation energy. The stabilization effect is similar to the case of boron, however, a bit more pronounced for Na and K (see Fig. 6). Similarly, the introduction of isovalent Sn impurities creates a distorted graphitic plain, which is again due to the increased atomic size of Sn and the significantly larger Sn-C bond length (from 1.43 Å to 2.05 Å). For this case, all AM atoms migrate to the top of the impurity, while they are at the center of a hexagon in the adjacent layer. Again, as in the previous cases, the AM intercalation results in a intercalant size dependent curvature of the system. The intercalation energy for Li, Na, and K amount to -1.91 eV, -1.93 eV, and -0.63 eV, thus showing the most pronounced stabilization of the intercalation process. When considering sulfur impurities, the S atom actually moves out of the graphitic plane, with the length of the S-C bonds amounting to 1.73Å. During intercalation, the curvature increases according to the AM atom sizes. However, while the Li atom remains in its original position at center of the honeycomb, Na and K atoms move to an off-center site (see Fig. 6). The intercalation energy for Li, Na, and K amount to -0.31 eV, -0.09 eV, 0.21 eV respectively, meaning that K intercalation remains unfavorable. Under intercalation, the S-C bonds increase slightly to 1.74 - 1.76 Å.

Finally, when regarding the OH impurity, already the intercalant-free system gets significantly curved with the maximal layer spacing increasing from 3.39 to 4.22 Å. This results in a decreased energetic penalty for AM intercalation and hence a large energetic stabilization for Li (-1.44 eV), Na (-1.09 eV), and K (-0.66 eV). While the Li atom travels to the f site, Na and K migrate to the d and g sites, respectively. These sites correspond to positions

on top of carbon atoms in the impurity plane and in the center of a hexagon of the second graphitic plane. It should be noted that adding OH impurities already causes a curvature in the system, which is further amplified when AM atoms are intercalated (see Fig. S6 in the SI). This increase is accompanied by changes in the O-C bond from 1.49 Å to 1.57 Å (1.60 Å and 1.60 Å) for Li (Na, and K), whereas the C-C bonds are only slightly affected ($\sim$ 1% variation).

Finally, to get additional insight, we compare the impact of impurities and typically observed structural defects. Interestingly, the impact of a mono-vacancy (MV) was found to result in a stabilization of the intercalation process that is similar to the Si and B impurities with the intercalation energies for Li, Na, and K amounting to -1.45 eV, -0.54 eV, and -0.33 eV, respectively.

Hence, a stabilization of the early stage intercalation, that is highly desirable for K (and Na) can be achieved by incorporating impurities or defects (or combinations thereof) into graphitic carbon. In this regard, it has to be pointed out that the stabilization of the early stage intercalation is desirable, however, a too strong bonding of AM atoms may also result in a permanent trapping of the latter ones, corresponding to irreversible capacity loss. Hence, the type of defects and impurities, as well as their ratio, is a critical factor that should be considered to optimize carbon based anode materials.

4 Conclusion

In this work, we have investigated the early stages of intercalation for Li, Na, and K in graphite-based model systems. Our findings reveal that the intercalation process for Li and K are fundamentally different. Due to the small size of Li ions, the intercalation process does not result in significant distortions of the graphitic planes and, moreover, makes it from the beginning energetically favorable. For K intercalation, on the other hand, the large ion size

results in significant distortions of the graphitic layers and a competition between vdW forces and covalent K-C bonds. This results in K-intercalation compounds with low K content being energetically unfavorable. In fact, only when a certain density of K atoms in between a graphitic layer is reached the compound becomes energetically favorable. To achieve this, the extremely low diffusion barriers for K in AB stacked graphite are highly beneficial. As a consequence, the initial steps for Li and K intercalation are different resulting in a random distribution of Li atoms, while K atoms prefer to fill one layer in a given graphitic domain. The differences in the energetics of the early stage intercalation may hence also explain the higher risk for plating and the increased resistance that is observed for KIBs with graphitic anodes. Furthermore, the energetics of the first intercalation steps may also hold as explanation for the sluggish kinetics, which is observed despite the fact that experimental and computational studies show lower diffusion barriers for K as compared to Li in graphite.[59–61] We furthermore, confirmed the lower diffusion barriers for K-GICs as compared to Li-GICs, which due to the large distortion caused by the K insertion seems counterintuitive at the first glance. However, these distortions are spatially extended, such that the spacing of the graphite atoms on neigbhouring planes is still strongly increased, which in turn facilitates the diffusion.

At last, we have investigated the impact of heteroatom doping on the energetics of the early stage intercalation process. These, along with defects, can stabilize the early stage K- (and also Na-) intercalation and may thus help to overcome limitations such as K-plating and sluggish kinetics in graphtic anodes. These findings, together with the gained insights in the differences of the intercalation processes may be applied for designing anode materials with improved performance.

Acknowledgement

This work contributes to the research performed at Cluster of Excellence EXC 2154 "Post-Li Storage", funded by the German Research Foundation (DFC). The authors acknowledge support by the state of Baden-Württemberg through bwHPC and the German Research Foundation (DFG) through grant no INST 40/575-1 FUGG (JUSTUS 2 cluster) and by the HoreKa supercomputer funded by the Ministry of Science, Research and the Arts Baden-Württemberg and by the Federal Ministry of Education and Research. This work contributes to the research performed at CELEST (Center for Electrochemical Energy Storage Ulm-Karlsruhe).

References

(1) Duong, D. L.; Yun, S. J.; Lee, Y. H. van der Waals layered materials: opportunities and challenges. *ACS nano* **2017**, *11*, 11803–11830.

(2) Zhao, W.; Zhao, C.; Wu, H.; Li, L.; Zhang, C. Progress, challenge and perspective of graphite-based anode materials for lithium batteries: A review. *Journal of Energy Storage* **2024**, *81*, 110409.

(3) May, A. F.; Yan, J.; McGuire, M. A. A practical guide for crystal growth of van der Waals layered materials. *J. Appl. Phys.* **2020**, *128*, 051101.

(4) Novoselov, K. S. Discovery of 2D van der Waals layered MoSi2N4 family. *National Science Review* **2020**, *7*, 1842–1844.

(5) Anji Reddy, M.; Helen, M.; Groß, A.; Fichtner, M.; Euchner, H. Insight into Sodium Insertion and the Storage Mechanism in Hard Carbon. *ACS Energy Lett.* **2018**, *3*, 2851–2857.

(6) Rana, K.; Sil, A.; Ray, S. Ball-Milled Graphite-Tin Composite Anode Materials for Lithium-Ion Battery. Materials Science Forum. 2013; pp 127–132.

(7) Karuppasamy, P.; Rajapanian, V. Transition Metal Dichalcogenide (TMD)-Based 2D Nanomaterials for Various Kinds of Rechargeable Batteries. *2D Nanomaterials: Synthesis, Properties and Applications* **2024**, 435–474.

(8) Engels, P.; Cerdas, F.; Dettmer, T.; Frey, C.; Hentschel, J.; Herrmann, C.; Mirfabrikikar, T.; Schueler, M. Life cycle assessment of natural graphite production for lithium-ion battery anodes based on industrial primary data. *Journal of Cleaner Production* **2022**, *336*, 130474.

(9) Luo, P.; Zheng, C.; He, J.; Tu, X.; Sun, W.; Pan, H.; Zhou, Y.; Rui, X.; Zhang, B.;

Huang, K. Structural engineering in graphite-based metal-ion batteries. *Advanced Functional Materials* **2022**, *32*, 2107277.

(10) Zhao, L.; Ding, B.; Qin, X.-Y.; Wang, Z.; Lv, W.; He, Y.-B.; Yang, Q.-H.; Kang, F. Revisiting the roles of natural graphite in ongoing lithium-ion batteries. *Advanced Materials* **2022**, *34*, 2106704.

(11) Charlier, J.-C.; Gonze, X.; Michenaud, J.-P. Graphite interplanar bonding: electronic delocalization and van der Waals interaction. *Europhysics letters* **1994**, *28*, 403.

(12) Horie, C.; Miyazaki, H. Atomic-force-microscopy images of graphite due to van der Waals interactions. *Physical Review B* **1990**, *42*, 11757.

(13) Zhang, H.; Yang, Y.; Ren, D.; Wang, L.; He, X. Graphite as anode materials: Fundamental mechanism, recent progress and advances. *Energy Storage Materials* **2021**, *36*, 147–170.

(14) Yang, Y.; Wang, J.; Du, X.; Jiang, H.; Du, A.; Ge, X.; Li, N.; Wang, H.; Zhang, Y.; Chen, Z.; Zhao, J.; Cui, G. Cation Co-Intercalation with Anions: The Origin of Low Capacities of Graphite Cathodes in Multivalent Electrolytes. *J. Am. Chem. Soc.* **2023**, *145*, 12093–12104.

(15) Guerard, D.; Herold, A. Intercalation of lithium into graphite and other carbons. *Carbon* **1975**, *13*, 337–345.

(16) Dahn, J. Phase diagram of Li x C 6. *Physical Review B* **1991**, *44*, 9170.

(17) Ohzuku, T.; Iwakoshi, Y.; Sawai, K. Formation of lithium-graphite intercalation compounds in nonaqueous electrolytes and their application as a negative electrode for a lithium ion (shuttlecock) cell. *Journal of The Electrochemical Society* **1993**, *140*, 2490.

(18) Fujimoto, H.; Mabuchi, A.; Tokumitsu, K.; Chinnasamy, N.; Kasuh, T. 7Li nuclear

magnetic resonance studies of hard carbon and graphite/hard carbon hybrid anode for Li ion battery. *Journal of Power Sources* **2011**, *196*, 1365–1370.

(19) Sanders, K. J.; Aguilera, A. R.; Keffer, J. R.; Balcom, B. J.; Halalay, I. C.; Goward, G. R. Transient lithium metal plating on graphite: Operando 7Li nuclear magnetic resonance investigation of a battery cell using a novel RF probe. *Carbon* **2022**, *189*, 377–385.

(20) Nonaka, T.; Kawaura, H.; Makimura, Y.; Nishimura, Y. F.; Dohmae, K. In situ X-ray Raman scattering spectroscopy of a graphite electrode for lithium-ion batteries. *Journal of Power Sources* **2019**, *419*, 203–207.

(21) Lenchuk, O.; Adelhelm, P.; Mollenhauer, D. New insights into the origin of unstable sodium graphite intercalation compounds. *Physical Chemistry Chemical Physics* **2019**, *21*, 19378–19390.

(22) Song, T.; Xie, Y.; Chen, Y.; Guo, H. Thermodynamics of graphite intercalation binary alloys of Li-Na, Na-K, and Li-K from van der Waals density functionals. *Journal of Solid State Electrochemistry* **2019**, *23*, 2825–2834.

(23) Kim, H.; Yoon, G.; Lim, K.; Kang, K. A comparative study of graphite electrodes using the co-intercalation phenomenon for rechargeable Li, Na and K batteries. *Chemical Communications* **2016**, *52*, 12618–12621.

(24) Jache, B.; Adelhelm, P. Use of graphite as a highly reversible electrode with superior cycle life for sodium-ion batteries by making use of co-intercalation phenomena. *Angewandte Chemie International Edition* **2014**, *53*, 10169–10173.

(25) Oka, H.; Makimura, Y.; Uyama, T.; Nonaka, T.; Kondo, Y.; Okuda, C. Changes in the stage structure of Li-intercalated graphite electrode at elevated temperatures. *Journal of Power Sources* **2021**, *482*, 228926.

(26) Holland, J.; Bhandari, A.; Kramer, D.; Milman, V.; Hanke, F.; Skylaris, C.-K. Ab initio study of lithium intercalation into a graphite nanoparticle. *Materials Advances* **2022**, *3*, 8469–8484.

(27) Liu, Q.; Li, S.; Wang, S.; Zhang, X.; Zhou, S.; Bai, Y.; Zheng, J.; Lu, X. Kinetically determined phase transition from stage II (LiC12) to stage I (LiC6) in a graphite anode for Li-ion batteries. *The Journal of Physical Chemistry Letters* **2018**, *9*, 5567–5573.

(28) Weng, S.; Wu, S.; Liu, Z.; Yang, G.; Liu, X.; Zhang, X.; Zhang, C.; Liu, Q.; Huang, Y.; Li, Y.; others Localized-domains staging structure and evolution in lithiated graphite. *Carbon Energy* **2023**, *5*, e224.

(29) Persson, K.; Hinuma, Y.; Meng, Y. S.; Van der Ven, A.; Ceder, G. Thermodynamic and kinetic properties of the Li-graphite system from first-principles calculations. *Physical Review B* **2010**, *82*, 125416.

(30) Persson, K.; Sethuraman, V. A.; Hardwick, L. J.; Hinuma, Y.; Meng, Y. S.; Van Der Ven, A.; Srinivasan, V.; Kostecki, R.; Ceder, G. Lithium diffusion in graphitic carbon. *The journal of physical chemistry letters* **2010**, *1*, 1176–1180.

(31) Onuma, H.; Kubota, K.; Muratsubaki, S.; Ota, W.; Shishkin, M.; Sato, H.; Yamashita, K.; Yasuno, S.; Komaba, S. Phase evolution of electrochemically potassium intercalated graphite. *J. Mater. Chem. A* **2021**, *9*, 11187–11200.

(32) Azizi, J.; Groß, A.; Euchner, H. Computational investigation of carbon based anode materials for Li-and post-Li ion batteries. *ChemSusChem* **2024**, e202301493.

(33) Moriwake, H.; Kuwabara, A.; Fisher, C. A.; Ikuhara, Y. Why is sodium-intercalated graphite unstable? *RSC advances* **2017**, *7*, 36550–36554.

(34) Euchner, H.; Vinayan, B. P.; Reddy, M. A.; Fichtner, M.; Groß, A. Alkali metal insertion

into hard carbon–the full picture. *Journal of Materials Chemistry A* **2020**, *8*, 14205–14213.

(35) Euchner, H.; Groß, A. Atomistic modeling of Li-and post-Li-ion batteries. *Physical Review Materials* **2022**, *6*, 040302.

(36) Jian, Z.; Luo, W.; Ji, X. Carbon electrodes for K-ion batteries. *Journal of the American chemical society* **2015**, *137*, 11566–11569.

(37) Luo, W.; Wan, J.; Ozdemir, B.; Bao, W.; Chen, Y.; Dai, J.; Lin, H.; Xu, Y.; Gu, F.; Barone, V.; others Potassium ion batteries with graphitic materials. *Nano letters* **2015**, *15*, 7671–7677.

(38) Komaba, S.; Hasegawa, T.; Dahbi, M.; Kubota, K. Potassium intercalation into graphite to realize high-voltage/high-power potassium-ion batteries and potassium-ion capacitors. *Electrochemistry Communications* **2015**, *60*, 172–175.

(39) Liu, J.; Yin, T.; Tian, B.; Zhang, B.; Qian, C.; Wang, Z.; Zhang, L.; Liang, P.; Chen, Z.; Yan, J.; others Unraveling the potassium storage mechanism in graphite foam. *Advanced Energy Materials* **2019**, *9*, 1900579.

(40) Kresse, G.; Furthmüller, J. Efficient iterative schemes for ab initio total-energy calculations using a plane-wave basis set. *Physical review B* **1996**, *54*, 11169.

(41) Kresse, G.; Joubert, D. From ultrasoft pseudopotentials to the projector augmented-wave method. *Physical review b* **1999**, *59*, 1758.

(42) Kresse, G.; Furthmüller, J. Efficiency of ab-initio total energy calculations for metals and semiconductors using a plane-wave basis set. *Computational materials science* **1996**, *6*, 15–50.

(43) Henkelman, G.; Jónsson, H. A dimer method for finding saddle points on high dimensional potential surfaces using only first derivatives. *The Journal of chemical physics* **1999**, *111*, 7010–7022.

(44) Henkelman, G.; Jónsson, H. Improved tangent estimate in the nudged elastic band method for finding minimum energy paths and saddle points. *The Journal of chemical physics* **2000**, *113*, 9978–9985.

(45) Jäckle, M.; Helmbrecht, K.; Smits, M.; Stottmeister, D.; Groß, A. Self-diffusion barriers: possible descriptors for dendrite growth in batteries? *Energy Environ. Sci.* **2018**, *11*, 3400–3407.

(46) Guo, M.; Zhang, H.; Huang, Z.; Li, W.; Zhang, D.; Gao, C.; Gao, F.; He, P.; Wang, J.; Chen, W.; Chen, X.; Terrones, M.; Wang, Y. Liquid Template Assisted Activation for "Egg Puf"-Like Hard Carbon toward High Sodium Storage Performance. *Small* **2023**, *19*, 2302583.

(47) Sahoo, R.; Tharigopala Vincent, B.; Thirugnamam, L.; Venkatachalam, S.; Sundara, R. Effect of Addition of Thermally Annealed Graphene in Tender Coconut-Derived Hard Carbon for Potassium Ion Battery. *ACS Appl. Energy Mater.* **2024**, *7*, 7006–7018.

(48) Esser, B.; Ehrenberg, H.; Fichtner, M.; Groß, A.; Janek, J. Post-Lithium Storage—Shaping the Future. *Adv. Energy Mater.* **2024**, 2402824.

(49) Xu, Z.; Lv, X.; Chen, J.; Jiang, L.; Lai, Y.; Li, J. Dispersion-corrected DFT investigation on defect chemistry and potassium migration in potassium-graphite intercalation compounds for potassium ion batteries anode materials. *Carbon* **2016**, *107*, 885–894.

(50) Thinius, S.; Islam, M. M.; Heitjans, P.; Bredow, T. Theoretical study of Li migration in lithium–graphite intercalation compounds with dispersion-corrected DFT methods. *The Journal of Physical Chemistry C* **2014**, *118*, 2273–2280.

(51) Yang, C.; Sun, X.; Zhang, X.; Li, J.; Ma, J.; Li, Y.; Xu, L.; Liu, S.; Yang, J.; Fang, S.; others Is graphite nanomesh a promising anode for the Na/K-Ions batteries? *Carbon* **2021**, *176*, 242–252.

(52) Olsson, E.; Chai, G.; Dove, M.; Cai, Q. Adsorption and migration of alkali metals (Li, Na, and K) on pristine and defective graphene surfaces. *Nanoscale* **2019**, *11*, 5274–5284.

(53) Wang, T.; Li, Q.; Feng, Q.; Miao, Y.; Li, T.; Qi, J.; Wei, F.; Meng, Q.; Ren, Y.; Xiao, B.; Xue, X.; Sui, Y.; Sun, Z. Carbon defects applied to potassium-ion batteries: a density functional theory investigation. *Nanoscale* **2021**, *13*, 13719–13734.

(54) Ling, C.; Mizuno, F. Boron-doped graphene as a promising anode for Na-ion batteries. *Physical Chemistry Chemical Physics* **2014**, *16*, 10419–10424.

(55) Yun, Y. S.; Le, V.-D.; Kim, H.; Chang, S.-J.; Baek, S. J.; Park, S.; Kim, B. H.; Kim, Y.-H.; Kang, K.; Jin, H.-J. Effects of sulfur doping on graphene-based nanosheets for use as anode materials in lithium-ion batteries. *Journal of Power Sources* **2014**, *262*, 79–85.

(56) Wu, J.; Cao, Y.; Zhao, H.; Mao, J.; Guo, Z. The critical role of carbon in marrying silicon and graphite anodes for high-energy lithium-ion batteries. *Carbon Energy* **2019**, *1*, 57–76.

(57) Wen, Y.; He, K.; Zhu, Y.; Han, F.; Xu, Y.; Matsuda, I.; Ishii, Y.; Cumings, J.; Wang, C. Expanded graphite as superior anode for sodium-ion batteries. *Nature communications* **2014**, *5*, 4033.

(58) Li, W.; Sun, X.; Yu, Y. Si-, Ge-, Sn-based anode materials for lithium-ion batteries: from structure design to electrochemical performance. *Small Methods* **2017**, *1*, 1600037.

(59) Wang, Z.; Ratvik, A. P.; Grande, T.; Selbach, S. M. Diffusion of alkali metals in the first stage graphite intercalation compounds by vdW-DFT calculations. *Rsc Advances* **2015**, *5*, 15985–15992.

(60) Olsson, E.; Chai, G.; Dove, M.; Cai, Q. Adsorption and migration of alkali metals (Li, Na, and K) on pristine and defective graphene surfaces. *Nanoscale* **2019**, *11*, 5274–5284.

(61) Xu, Z.; Lv, X.; Chen, J.; Jiang, L.; Lai, Y.; Li, J. Dispersion-corrected DFT investigation on defect chemistry and potassium migration in potassium-graphite intercalation compounds for potassium ion batteries anode materials. *Carbon* **2016**, *107*, 885–894.

TOC Graphic